PRIFYSGOL ABERYSTWYTH UNIVERSITY

Aberystwyth University

Observational Aspects of the Three-dimensional Coronal Structure Over a Solar Activity Cycle

Morgan, Huw; Habbal, Shadia Rifai

Published in:
Astrophysical Journal

DOI:
10.1088/0004-637X/710/1/1

Publication date:
2010

Citation for published version (APA):
Morgan, H., & Habbal, S. R. (2010). Observational Aspects of the Three-dimensional Coronal Structure Over a Solar Activity Cycle. *Astrophysical Journal*, *710*(1), 1-15. https://doi.org/10.1088/0004-637X/710/1/1

General rights
Copyright and moral rights for the publications made accessible in the Aberystwyth Research Portal (the Institutional Repository) are retained by the authors and/or other copyright owners and it is a condition of accessing publications that users recognise and abide by the legal requirements associated with these rights.

• Users may download and print one copy of any publication from the Aberystwyth Research Portal for the purpose of private study or research.
• You may not further distribute the material or use it for any profit-making activity or commercial gain
• You may freely distribute the URL identifying the publication in the Aberystwyth Research Portal

Take down policy
If you believe that this document breaches copyright please contact us providing details, and we will remove access to the work immediately and investigate your claim.

tel: +44 1970 62 2400
email: is@aber.ac.uk

Download date: 05. May. 2023

The Astrophysical Journal, 710:1–15, 2010 February 10 doi:10.1088/0004-637X/710/1/1
© 2010. The American Astronomical Society. All rights reserved. Printed in the U.S.A.

OBSERVATIONAL ASPECTS OF THE THREE-DIMENSIONAL CORONAL STRUCTURE OVER A SOLAR ACTIVITY CYCLE

Huw Morgan and Shadia Rifai Habbal
Institute for Astronomy, University of Hawaii, 2680 Woodlawn Drive, Honolulu, HI 96822, USA; hmorgan@ifa.hawaii.edu
Received 2009 September 12; accepted 2009 November 26; published 2010 January 14

ABSTRACT

Solar rotational tomography is applied to almost eleven years of Large Angle Spectrometric Coronagraph C2/*Solar and Heliospheric Observatory* data, revealing for the first time the behavior of the large-scale coronal density structures, also known as streamers, over almost a full solar activity cycle. This study gives an overview of the main results of this project. (1) Streamers are most often shaped as extended, narrow plasma sheets. The sheets can be extremely narrow at times ($\leqslant 0.14 \times 10^6$ km at 4 $R_\odot$). This is over twice their heliocentric angular thickness at 1 AU. (2) At most times outside the height of solar maximum, there are two separate stable large helmet streamer belts extending from mid-latitudes (in both north and south). At solar minimum, the streamers converge and join near the equator, giving the impression of a single large helmet streamer. Outside of solar minimum, the two streamers do not join, forming separate high-density sheets in the extended corona (one in the north, another in the south). At solar maximum, streamers rise radially from their source regions, while during the ascending and descending activity phases, streamers are skewed toward the equator. (3) For most of the activity cycle, streamers share the same latitudinal extent as filaments on the disk, showing that large-scale stable streamers are closely linked to the same large-scale photospheric magnetic configuration, which give rise to large filaments. (4) The poleward footpoints of the streamers are often above crown polar filaments and the equatorial footpoints are above filaments or active regions (or above the photospheric neutral lines which underlie these structures). The high-density structures arising from the equatorial active regions either rise and form the equatorial footpoints of mid-latitude quiescent streamers, or form unstable streamers at the equator, not connected to the quiescent streamer structure at higher latitude (so there are often three streamer sheets sharing the same extended longitudinal region). (5) Comparison between the tomography results and a potential field source surface model shows that streamers are not necessarily associated with a magnetic polarity reversal, but rather are regions containing field lines arising from widely separated sources at the Sun. We call these convergence sheets. (6) There is considerable differential rotation of streamers at high latitudes, which makes comparison between disk and coronal structure complicated. The presence of differential rotation has implications for many areas of coronal and heliospheric research.

Key words: Sun: corona – Sun: filaments, prominences – Sun: rotation – solar wind

1. INTRODUCTION

It has been known for over a century that the shape of the corona, as defined by the appearance of streamers in white-light observations made during total solar eclipses, or with coronagraphs, changes with the solar cycle (Loucif & Koutchmy 1989). At the minimum solar activity, streamers seem to be confined to low latitudes. At solar maximum, their distribution is almost circularly symmetric. Such a change in distribution with the solar cycle seems counterintuitive if one considers a likely connection with active regions. The latter, which are directly linked to the emergence of sunspots, follow the opposite pattern, emerging at $\pm 30^\circ$ at solar minimum and migrating toward the equator at solar maximum, thus producing the well-known butterfly diagram (Carrington 1858; Maunder 1922). Hence, establishing the sources of streamers at the Sun is essential for understanding how the solar magnetic field expands outward from the photosphere, and how it impacts the solar wind flow.

It seems that large polar coronal holes are unambiguously connected to the fast, low-density solar wind. There remains uncertainty, however, as to the source of the slow, higher density solar wind that forms streamers in coronagraph observations. Most recent studies, which attempt to address this question, are based on a combination of potential field source surface (PFSS) models with observations of the inner corona by eclipse or coronagraph (Ambrož et al. 2009; Koutchmy et al. 2001), and/or in situ measurements of the solar wind far from the Sun (Wang & Sheeley 1990; Lepri et al. 2008, for example). PFSS models are extrapolations of the observed photospheric magnetic field into the corona under certain boundary conditions, thus giving an estimate of the large-scale magnetic field between the photosphere and a source surface (typically placed at a height of approximately 3 $R_\odot$; Altschuler & Newkirk 1969; Schatten et al. 1969; Wang & Sheeley 1992). Neugebauer et al. (2002) ballistically mapped the path of different solar wind streams measured by *Ulysses* (Wenzel et al. 1992) and *ACE* (*Advanced Composition Explorer*; Stone et al. 1998) back to a source surface, then used a PFSS model to trace the source of the various streams back to either coronal holes or active regions at the Sun. Leamon & McIntosh (2009) is a more recent similar study, concentrating on "magnetic regions of influence" at the Sun, which segments the photosphere into open and closed regions (McIntosh et al. 2006). Using spectral observations by the UltraViolet Coronagraph Spectrometer (UVCS; Kohl et al. 1995), Susino et al. (2008) analyzed coronal outflow velocities and temperatures along the boundary of a streamer, and found the slowest wind at the streamer center (along the cusp), with slow wind at the boundary. Unfortunately, no detailed analysis of the structures lying at the base of the streamer was made. Ko et al. (2008) combined synoptic maps by the Extreme UltraViolet Imaging Telescope (EIT; Delaboudiniere et al. 1995) and Large Angle Spectrometric Coronagraph (LASCO; Brueckner et al.

1995) with UVCS observations and a magnetohydrodynamic (MHD) model to study the link between coronal structure and magnetic field at the Sun.

Many studies of the solar wind sources at the Sun are concerned with coronal holes and active regions, with little mention of filaments (prominences) as contributors to the solar wind. In contrast, Uzzo et al. (2006) make a detailed study of a structure that they describe as a quiescent streamer arising from a complex collection of filaments. Morgan & Habbal (2007a) used a comparison between a simple density model and coronagraph images to show that much or the streamer structure in the north coronal hemisphere during 2003 July and August must arise from filaments, or the magnetic distribution underlying the filaments. Habbal et al. (2007) ascribe the footpoints of several streamers observed during the 2006 total solar eclipse to filaments. Zhukov et al. (2008) shows that polar streamers are closely associated with what they call the "polar neutral lines" where the crown polar filaments lie, and are latitudinally centered above these lines at solar maximum.

PFSS extrapolations are often used as a proxy for coronal density structure (Wang et al. 1997). The most commonly used interpretation of the magnetic field map at the source surface is that high-density streamers are expected to lie mostly along the neutral line of the heliospheric current sheet (HCS). However, studies have shown that streamers can lie elsewhere in the corona (Saez et al. 2005; Morgan & Habbal 2007a). Wang et al. (2007) presented a more general and correct interpretation of PFSS, that streamers lie along the HCS, and that "pseudostreamers" lie along regions where magnetic field lines have emerged from widely separated latitudes at the Sun.

Global MHD models use the magnetic field structure given by PFSS, along with other properties such as density, temperature, and outflow velocity, as initial conditions. The steady-state solutions reached by these models give an estimate of the density as well as other properties of the corona (Mikic et al. 1996; Usmanov 1996; Linker et al. 1999). These models also show that not all streamers are restricted to the HCS.

In addition to the great instrumental challenges of observing the faint corona, there are many difficulties in using coronal data to establish the coronal structure, and to analyze the source of structures at the Sun. Coronagraph (and eclipse) observations are dominated by the steep radial gradient in brightness. In order to view the structure in such images, it is necessary to remove the radial gradient to enhance the latitudinal gradients. Morgan et al. (2006) introduced the Normalizing Radial Graded Filter (NRGF), which enables not just a continuous view of structure through a single coronagraph observation, but a smooth continuation of structure between observations made by different instruments. This enables an effective tracing of coronal structures from large to small heights. Other image processing techniques are aiding in the structural analysis of eclipse and coronagraph data (Ambrož et al. 2009; Pasachoff et al. 2009). Contemporary coronagraphs are ineffective at looking at the very innermost corona (below $\sim$1.25 $R_{\odot}$), and this is a large hindrance in establishing links between the corona and Sun. While EUV observations (by EIT, for example) do reveal the corona below this height, the observation is in temperature-dependent spectral lines, which prevents a coherent continuation of structure from white-light coronagraph images down to the chromosphere. However, studies such as Frazin et al. (2005) have made inroads in structurally analyzing such data.

Another major challenge is in finding the distribution of three-dimensional (3D) density structure from two-dimensional (2D) coronagraph observations (i.e., resolving the line of sight). White-light coronagraph observations are dominated by the Thomson-scattered disk emission by coronal electrons—the brightness is therefore proportional to the integrated electron density along a line of sight. The most basic technique is to assume a simple geometry for the corona (for example, spherical symmetry), and to invert the observed brightness directly (van de Hulst 1950; Saito et al. 1977; Quémerais & Lamy 2002). This robust technique is a reasonable approach when the corona possesses a simple geometry, for example, at the minimum of solar activity the assumption of a spherical or cylindrical symmetry is a good approximation, particularly over the poles. Refined estimates may be made by assuming more sophisticated geometries (Guhathakurta et al. 1996; Gibson et al. 2003). Using the estimated position of the HCS as a constraint on the spatial position of structure, density may be calculated from *pB* coronagraph observations, leading in particular to a refined estimate of the electron density of streamers (Thernisien & Howard 2006; Saez et al. 2007). However, such studies are based on the assumption that the position of the HCS as determined by PFSS is accurate.

A series of images made of the corona over a solar rotation shows a steadily changing appearance. This variation can be exploited by assuming it is solely due to the rotation of the corona, and a 3D reconstruction of the coronal density distribution may be built. This approach is called Solar Rotational Tomography (SRT; see Frazin 2000, and references within). For studying the large-scale coronal structure, SRT is superior to the more commonly used Carrington maps of white-light brightness, since the tomography resolves the distribution of density along the line of sight. Therefore, the true latitude, longitude, and shape of structures are found. Morgan et al. (2009) describe a new SRT approach based on Fourier backprojection tomography of normalized white-light coronagraph observations. Since the data are normalized prior to backprojection, the resulting maps give a qualitative rather than quantitative picture of coronal structure, thus the technique is called Qualitative SRT (QSRT). The normalizing of the data is achieved using the NRGF (Morgan et al. 2006). Despite the qualitative nature of the maps, they are useful for analyzing the distribution of streamers within the corona. That is, they show where high-density structures lie, but they cannot yet give the absolute value of electron density. Morgan et al. (2009) applied the technique successfully to LASCO C2 data covering a period of one half-rotation bridging Carrington rotations (CRs) 2000 and 2001 (2003/03/16 to 2003/03/31). The same techniques are applied in this work to a series of LASCO C2 observations covering almost a whole solar activity cycle. This article presents an overview of the main findings of this study.

The method is presented in Section 2. Results with relevant discussion are organized in the following sections:

1. Confirmation of streamers as very narrow extended sheets (Section 3).
2. Case studies of selected CRs over the activity cycle (Section 4).
3. Comparison of butterfly diagrams for coronal streamers, active regions, and filaments (Section 5).
4. Discussion of the link between disk and coronal structure (Section 6).
5. Comparison of a large-scale magnetic field model and the tomography (Section 7).
6. Evidence of the coronal differential rotation (Section 8).

Conclusions are given in Section 9, and an overview of future work is given in Section 10.

2. METHOD

The period we choose starts at CR1914 and ends with CR2058 (1996/10 to 2007/07). The aim is to create a reconstruction density map for each CR over this almost 11 year period. For each CR, a period of approximately two weeks (half a solar rotation as observed from Earth), is identified. The time period is centered at the midpoint of the CR (the time at which the meridional Carrington longitude is 180°). For each half-rotation period, LASCO C2 total brightness (B_t) and polarized brightness (pB) observations are downloaded and processed according to the techniques described in Morgan et al. (2009). For efficiency, approximately one observation every 2 hr (usually one in every four or five observations), is used. If there are excessive gaps in the data, or an obvious error in the reconstructed density map, the half-rotation time period is shifted (but still within the same CR) and a different set of data processed. There are some rotations where excessive data gaps are unavoidable, or for other reasons the reconstruction is obviously in error. However, successful reconstructions are obtained for most rotations over the activity cycle.

While there is no rigorous way of testing the accuracy of a particular reconstruction, synthetic observations created from the reconstructed densities can be compared with the true observations. Good agreement between synthetic and true observations over the period of half-rotation gives reasonable confidence in the accuracy of the reconstruction. An example is shown in Figure 1. Morgan et al. (2009) give details on how synthetic observations are created from the reconstructed densities. Figure 1(a) shows the reconstructed density map for CR1931 (1998/01). High densities are restricted to a narrow band near to the equator, with the band slowly varying in latitude from $\sim -20°$ to $+10°$. This is the main equatorial streamer belt. A tongue of lower density structure lies northward of the main streamer belt extending between longitudes $\sim$100° and 235°. This tongue seems to join the main streamer belt at longitude 235°. Synoptic maps of observed and synthetic brightness are compared in Figure 1(b). These maps show that the distribution of the reconstructed streamer belt is accurate. Figure 1(c) shows three sets of observed and synthetic images for three different observation times during CR1931. The low-density streamer labeled "S" in part (ii), seen in both observed and synthetic images, is created by the end of the lower density tongue at longitude 100°. The blotchy appearance of the north and south coronal holes in the reconstruction density map are caused by errors and true rapid temporal changes in the corona. For example, Figure 1(c) (i) shows a large observed coronal mass ejection (CME) in the northeast. The CME is a rapid change in brightness in a restricted region, observed in only one image (recall that only one observation every 2 hr is used), so does not have a devastating effect on the reconstructed density. It does however lead to some error, and this is most clearly seen in the large areas of low density in the coronal holes. There are three large CMEs observed during the half-rotation period, as can be seen in the observed synoptic map of Figure 1(b). The regions of low densities which hug the north edge of the tongue structure (of even lower densities than the poles) are an undesirable side-effect of applying tomography to normalized data. The quality of the reconstruction shown in this example is typical of most reconstructions over the activity cycle. Some appear cleaner, with less noise in low-density regions. At solar

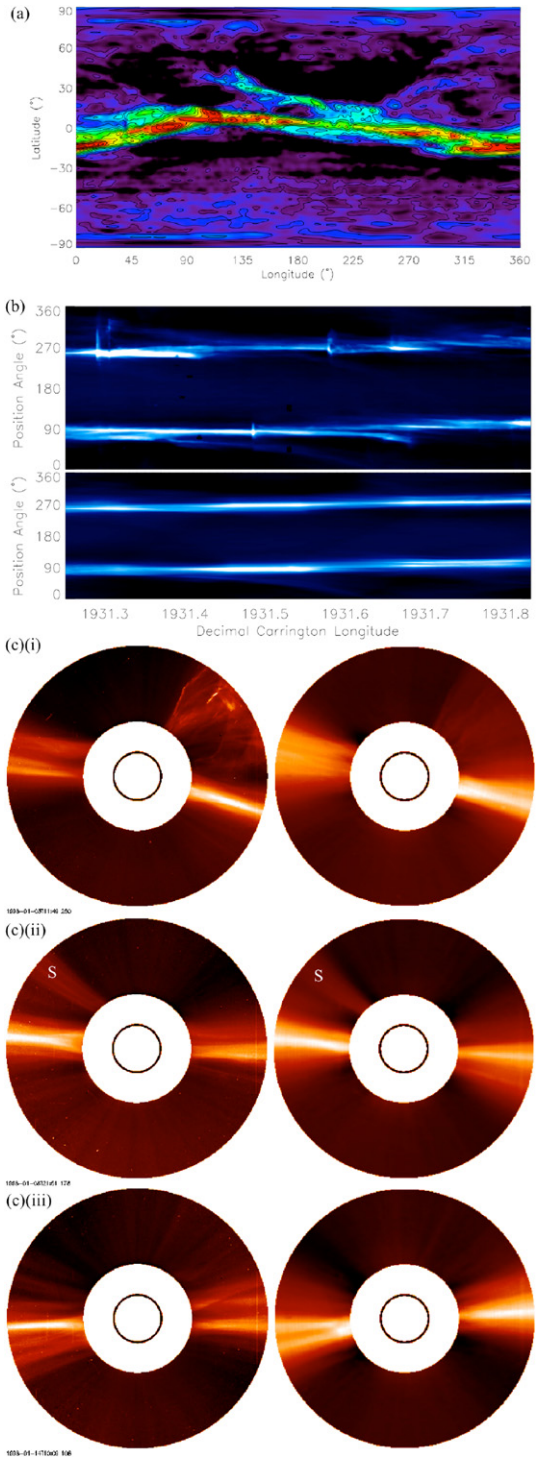

Figure 1. (a) Longitude–latitude map of the coronal density distribution at a height of 4 $R_\odot$ determined using the QSRT technique for LASCO C2 data observed during the period 1998/01/02 to 1998/01/15. Red is high density, and black is low (arbitrary units). For clarity, a small smoothing window (of width $3° \times 3°$) has been applied. (b) Synoptic maps of the corona for the whole observational period. The maps are constructed from latitudinal profiles at a height of 4 $R_\odot$, stacked in time from left to right. The vertical axis is position angle, or angle counterclockwise from north. The horizontal axis shows decimal Carrington Longitude at the meridian. The top plot is the observed synoptic map, the bottom is a synthetic map created from the QSRT reconstruction. (c) Comparison of observations (left column) with synthetic observations created from the QSRT reconstruction (right column). The three observation-model pairs are for different dates, from top to bottom: 1998/01/03, 1998/01/08, and 1998/01/14. These dates correspond to meridional Carrington longitudes of 250°, 178°, and 108°. The inner ring in all images shows the position of the Sun. The field of view is 2.6–6 $R_\odot$. All images are processed with the NRGF.

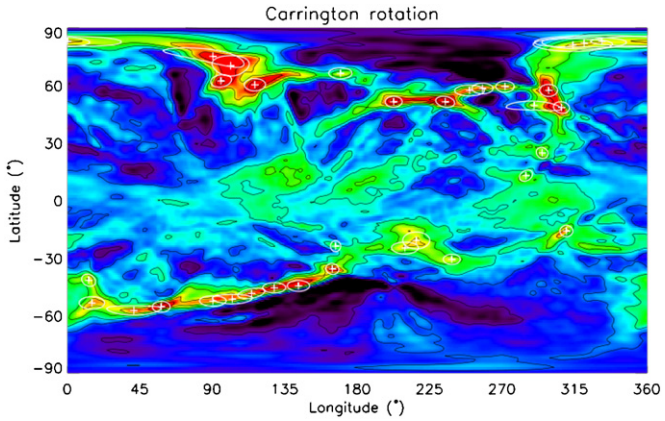

Figure 2. Longitude–latitude map of the coronal density distribution at a height of 4 $R_\odot$ determined using LASCO C2 data observed during the period 1999/07/28 to 1999/08/11. White crosses show the position of high-density peaks as detected by the procedure described in Section 5. The white ovals surrounding the high-density peaks show a Gaussian profile fit to the density peaks, not used for this study.

maximum, CMEs occur more frequently (perhaps several a day), and low-density regions can be very noisy. Despite this, the maps show the position of high-density streamers unambiguously.

For the statistical study of Section 5, an automated procedure is used to detect the position of high-density peaks in the reconstruction maps. The following list describes the procedure.

1. A 2D longitude–latitude map, such as that shown in Figure 1(a), is extended (or "wrapped"), around longitude, so that the longitudinal axis of the map extends from −45° to 405°. The map has a resolution of around 1° longitude by 1° latitude per pixel.
2. An "a trous" wavelet decomposition (Starck et al. 1998) is made of the extended 2D map. This gives a set of maps showing features from highest to lowest spatial frequency.
3. Maxima in each level of the decomposition are identified. In the highest frequency map, there are hundreds of small peaks, but most of these are caused by noise. At the lowest frequency, very few peaks are present. Overall positions of maxima in the original map are defined as points where maxima exist at all decomposed levels from the highest frequency to the third lowest frequency. From one decomposition level to the next, the position of the maxima may vary by a pixel or two.
4. Finally, those maxima that have a "density" in the top 20% of the original map are identified as the position of a high-density streamer.

As an example, Figure 2 shows a reconstruction map for CR1952 (1999/08), with the peaks of streamers identified by white crosses and circles using the procedure described above. Firstly, what is evident in this density map is the high level of noise in low-density regions. This can be compared with the noise level in the coronal holes of Figure 1(a). The increased noise in this map is probably caused by the increased frequency of CMEs during the observational period. Secondly, within an extended high-density structure (for example, the long and narrow streamer extending from longitude 0° to 180° at mid-latitudes in the south), the procedure detects many individual peaks. It is likely that the corona exhibits this behavior—that large-scale streamers contain considerable finer scale structure (see, for example, Thernisien & Howard 2006 or Morgan & Habbal 2007b), although it is unknown if such fine-scale

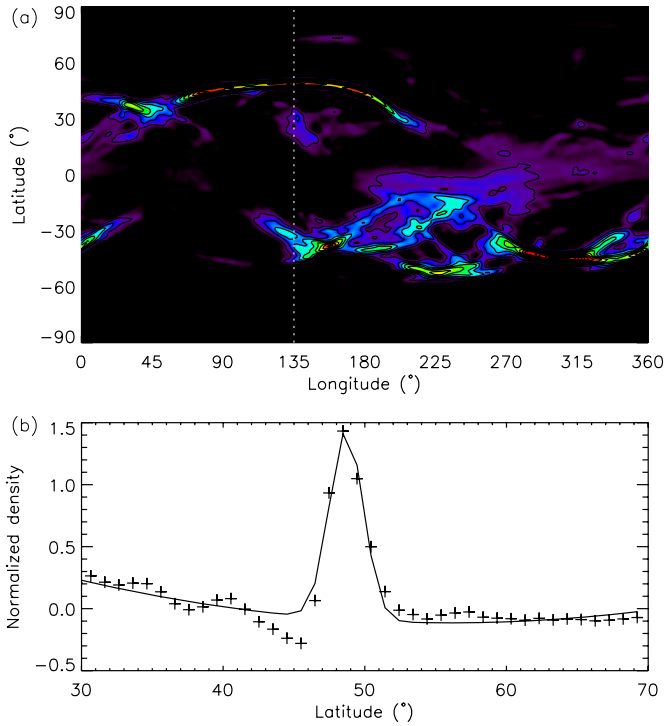

Figure 3. (a) Tomography map for CR2010. The vertical dotted white line is at longitude 135°, where a slice through the map is taken for further analysis. (b) The slice of normalized density from the tomography map at longitude 135°, plotted against latitude between 30° and 70°, is shown as crosses. A fit to a 2nd degree polynomial and a Gaussian is shown as the solid line.

structure would remain stable for a long enough period to show up in the tomography reconstructions. Some of the multiple peaks detected by this procedure may be the superposition of noise on the reconstructed density. What is important is that the procedure detects accurately the position of the streamer, and if it does this through detecting multiple peaks within a streamer rather than the main highest density peak, is not so important for this study.

Many of the tomography maps shown in this paper also map the positions of filaments and active regions, as observed by ground-based instruments. The active region data is extracted from the Solar Region Summary reports, prepared jointly by the US Department of Commerce, NOAA, Space Weather Prediction Center and the US Air Force from data received by the Space Weather Operations branch of NOAA. The filament data is provided by L'Observatoire Paris Meudon.

3. STREAMERS AS HIGH-DENSITY SHEETS

Figure 3(a) shows a particularly clean reconstruction made for a quiet descending stage in the solar cycle—CR2010 (2003/12). The density map reveals streamers as extended narrow sheets of high density. Section 7 shows that some of these sheets can be associated with the HCS estimated by a PFSS model, while the others arise from an alternative interpretation of PFSS. For the streamers to appear so narrow and clean in the reconstruction means that they have remained very stable over the half-rotation period during which observations for the reconstruction were made. Any movement would result in a smearing of the density through the map, and a widening of the streamer sheets.

The most extended, narrow sheet describes a curve at mid-latitude in the north corona between longitudes of ∼45° and 225°. This sheet, as will be shown in Section 7, is firmly

associated with the HCS. For all the density maps created over the 11 year period, this streamer is one of the narrowest observed. Figure 3(b) shows a cross section of the streamer sheet, taken at a longitude of 135°. Fitting the streamer sheet to a Gaussian gives a full width at half-maximum (FWHM) of 2.°8 latitude. For the reconstruction at a height of 4 $R_\odot$, this translates into a thickness of 0.14×10^6 km at that height. This value then is an upper limit to the narrowest streamer found in our results. The true streamer is likely narrower, and cannot be thicker. Other streamers found in our results appear thicker than this one, but it is entirely possible that they appear so due to reconstruction error (for example, a change in the position of the streamer in time would result in a reconstruction showing a thicker streamer). Richie-Halford et al. (2009) estimated a thickness for the plasma sheet associated with the HCS of 3×10^6 km at 0.11 AU, corresponding to a heliocentric angular thickness of around 10°, using Cassini radio measurements during 2001–2002. This is far thicker than the one example shown here using the tomography maps; however, as stated previously, we do find much thicker plasma sheets. Using data from *ACE* during 2003, and *Ulysses* during 1991 and 2004, Zhou et al. (2005) found plasma sheet thickness of 3.08, 2.11, and 1.38×10^6 km at 1, 3, and 5 AU, respectively, corresponding to angular thicknesses of 1.°18, 0.°27, and 0.°11. The 1 AU thickness of Zhou et al. (2005) agrees well with that of Richie-Halford et al. (2009). The fact that we find a larger angular thickness to the plasma sheet close to the Sun is consistent with the general narrowing of the plasma sheet with height measured in the heliosphere.

4. CASE STUDIES

This section presents several specific CRs over the activity cycle as examples, and compares tomography density maps with processed composite images of the corona. The processed images show nested observations from the disk to the extended corona, and therefore a continuation of structure from the low to high corona. The tomography map, created for a height of 4 $R_\odot$, helps interpret the often complicated features seen in the coronal images. The coronal images help to determine which disk features can be associated with coronal streamers, and the overall configuration of the streamer with height can be studied.

4.1. CR1912, CR1922, and CR1927: Solar Minimum

Figure 4 shows a typical solar minimum corona, from CR1912 (1996/08). During this time, as can be seen in the figures of Section 5, the coronal streamers are restricted to a narrow range of latitudes surrounding the equator while filaments are at bands of a higher latitude, at ±50° from the equator. Active regions can be in two separated regions—either at ±30°, or close to the equator. The east limb of the coronal image of Figure 4(a) is the classic solar minimum configuration. Filaments, or the photospheric neutral lines associated with filaments, form the poleward footpoints of a large helmet streamer which straddles the equator. There is no obvious disk feature at the equator directly underlying the streamer cusp. At the west limb there are two plasma sheets sharing the same extended range of longitude. These two plasma sheets are two distinct streamers both of which lie above a chain of filaments running north–south. High-latitude filaments lie at the poleward footpoints of the streamers, while filaments and active regions form the equatorial footpoints. The two streamers do not extend radially outward from their footpoints. Despite being linear (i.e., follow a straight line in the extended corona), they lean toward the equator. This configuration of two plasma sheets approximately centered at longitude 270° during CR1912 lasts for many rotations. It disappears by CR1921, coinciding with the disappearance of the underlying chain of filaments. The dual plasma sheet structural configuration near longitude 270° has been described and discussed in detail by Saez et al. (2005).

During CR1921–CR1922 (1997/04 to 1997/05), the streamers are limited to a very narrow latitudinal extent around the equator, as can be seen in Figure 4(b). Despite this, the equatorial plasma sheet shows a weak splitting around longitude 225°, as can be seen clearly at the west limb of the coronal image or from the tomographic map. At the east limb, the single equatorial plasma sheet is narrow, but seems to arise from a joining of two separate helmet streamers with their broad footpoints centered at mid-latitude. This is most clearly seen in the composite coronal image, where a dark cavity lies at the equator at heights below 2 $R_\odot$, that is, at heights below where the two mid-latitude streamers have merged. As is typical of the examples shown in this work, the poleward footpoints of the streamers overlie the crown polar filaments, while the equatorial footpoints overlie equatorial filaments and/or active regions.

The equatorial plasma sheet configuration of CR1922 does not last long. By CR1927 (1997/09), the plasma sheet has split, at several regions of extended longitude. This is shown in Figure 4(c). The composite image shows multiple streamers arising from mid- and low latitudes at both limbs, corresponding to the multiple plasma sheets seen in the tomography map. Again, the mid-latitude streamers do not follow radial lines from their sources at the Sun. At low heights, the streamers curve in toward the equator. Above ∼2 $R_\odot$, they become linear but lean toward the equator. Despite the splitting, there is an extended longitudinal region near 180° where there remains a single plasma sheet at the equator. It is as if some longitudinal regions have maintained a typical solar minimum configuration (quadrupole, dipole, and current sheet configuration; see, for example, Banaszkiewicz et al. 1998), while in others the corona has started a transformation toward a more radial solar maximum configuration, with the dipole component weakened.

4.2. CR1931–CR1934: From Minimum to Maximum

Figure 5 shows four sets of density maps for CR1931, CR1932, CR1933, and CR1934 (1998/01 to 1998/04). CR1931 has, more or less, a single plasma sheet which meanders in latitude between −20° and +10°. The extended tongue of low density hanging north of the main equatorial plasma sheet between longitudes 135° and 235° leads to the narrow streamer seen rising from the northeast in the coronal image. This streamer appears to have an extreme curvature toward the equator at low heights. The main plasma sheet is tilted from the equator, causing a tilted appearance to the main streamers in the coronal image at both limbs. By CR1932, the main shape of the plasma sheet is similar to that of CR1931, although extended regions have split into separate north and south plasma sheets. This is very clear between longitudes 0° and 135°, and is hinted at near 270°. CR1933 is similar to CR1932, but with even further splitting at all longitudes. A feature of CR1933 is that there are several faint streamers rising at high latitude in the coronal image without corresponding structure in the tomographic map. A good example is in the southwest of the coronal image. These faint streamers seem to rise from the highest latitude filaments, and they probably are a rapidly changing feature of the corona during this period. Due to

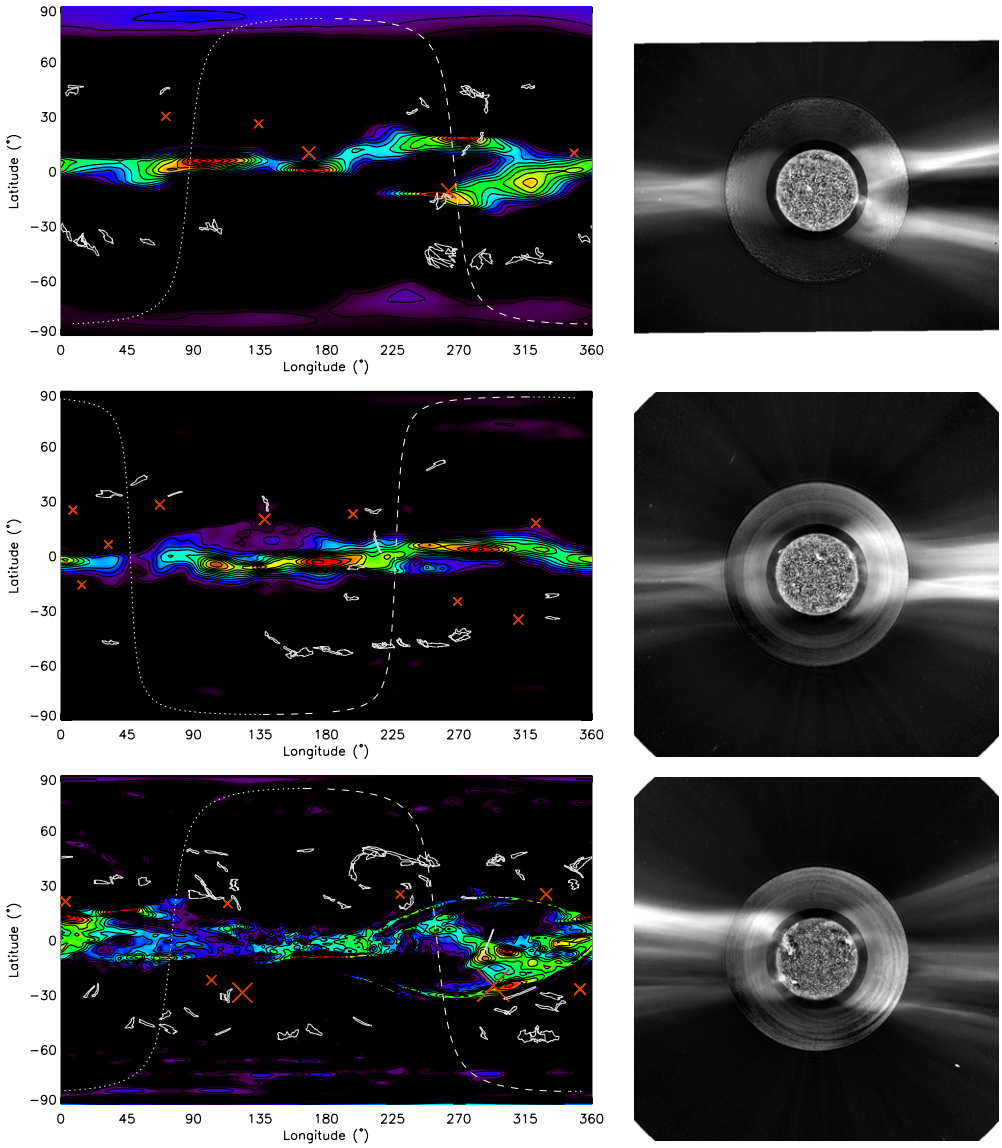

Figure 4. Density maps (left column) and coronal composite images (right column) for CR1912 (top), CR1922 (middle), and CR1927 (bottom). The composite image shows the corona at a particular date during the corresponding rotation. The density map is in Carrington longitude–latitude coordinates, with red as high density, black as low. Red crosses show positions of sunspots and white contours show filaments. To help interpret the coronal images on the right, the dashed (dotted) white line in the density map shows the position of the west (east) limb at the observation time of the coronal image. The inner part of the coronal images is an EIT/*SOHO* 304 Å observation. The lower corona is a Mauna Loa Solar Observatory (MLSO) MKIII coronameter observation, and the higher corona is LASCO C2.

the rapid change, the tomography does not reconstruct these features. By CR1934, there is an advanced splitting of the plasma sheet—there are two separate plasma sheets in both north and south, as well as low-density structures over the south pole. The coronal image suddenly appears very much like a solar maximum-type image compared to the previous three rotations.

4.3. CR1943 and CR1948: Streamers at Increasing Latitude

Figure 6 shows the coronal structure for CR1943 (1998/12). In the north, streamers lie at similar, or higher, latitudes than the northernmost filaments. In the south, streamers still lie somewhat closer to the equator than filaments. The east limb of the coronal image is very interesting. Three main streamers can be seen above this limb, corresponding to the three plasma sheets in the density map. The three sheets share the same longitudinal region, extending almost halfway around the Sun. One is centered above the equator, the other two at mid-latitudes. The equatorial plasma sheet may well be associated with a chain of large active regions situated just north of the equator at longitudes ∼90°–180°. The south plasma sheet seems to lie between two chains of filaments. In the north, at the west limb, there are filaments lying under the streamers—although there are also large, extended plasma sheets lying above regions where there are no filaments. The mid-latitude streamers overlying the filaments are seen in the coronal image to be helmet streamers extending approximately radially from their source regions. The equatorial streamer is not a helmet streamer, but is a bright fan-shaped streamer associated with the active region chain. This is reminiscent of the case studied in Morgan & Habbal (2007b). The bottom plot of Figure 6 shows the density configuration for CR1948 (1999/04). Mid-latitude streamers are again approximately centered over filaments. Both the coronal image and the tomographic map show an absence of streamers arising from the equatorial regions, corresponding possibly to the small number of active regions. A band of filaments at

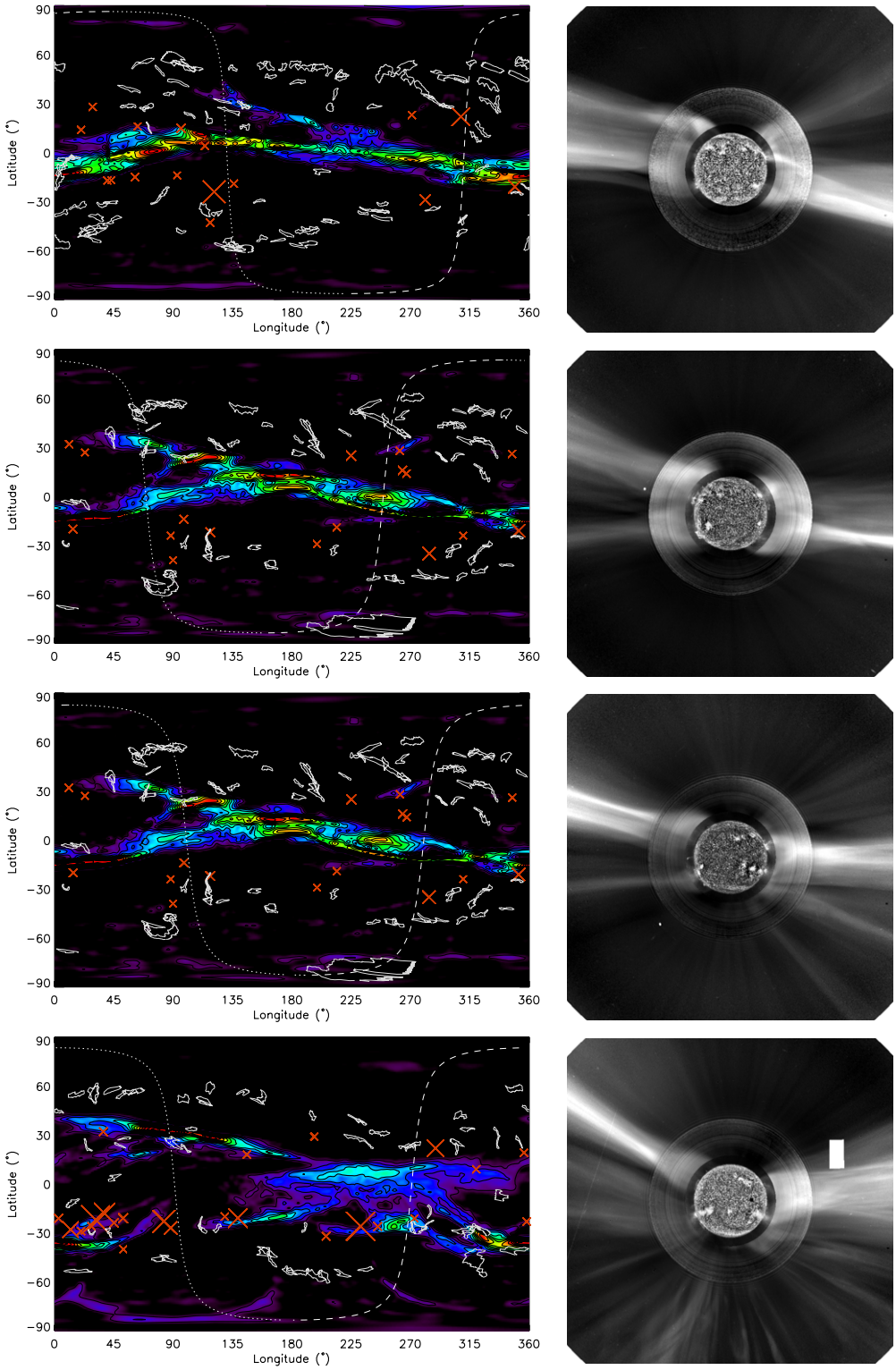

Figure 5. As Figure 4, but for (top to bottom) CR1931, CR1932, CR1933, and CR1934.

high latitude in the south corona, extending from ∼270° to 90° (wrapping around the 360°), do not lie under the streamers.

4.4. CR1961 and CR1970: Height of Solar Maximum

The streamer butterfly diagram of Section 5 shows streamers reaching the north pole during CR1961 (2000/04), and the south pole during CR1970 (2000/12). The density maps for these two times are shown in Figure 7. During CR1961, a ring of filaments surround the north pole at a latitude of ∼10°. A band of high-density cuts across the pole, with no correlation between its extended, straight, profile, and the shape of the circular ring of filaments lying underneath. This is in complete contrast to the south pole, which has a circular ring of filaments lying almost directly underneath a similarly shaped plasma sheet. By CR1970, the filaments have retreated rapidly from the north pole (this jump can be seen in the butterfly diagram of Figure 9(c)),

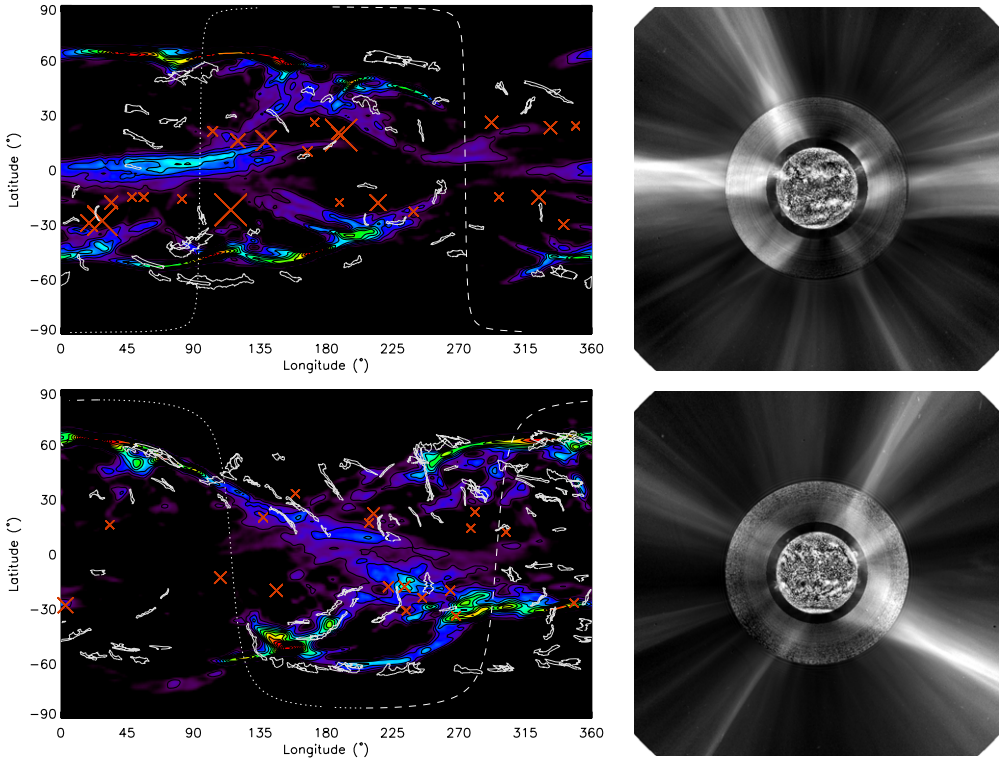

Figure 6. As Figure 4, but for CR1943 (top), and CR1948 (bottom).

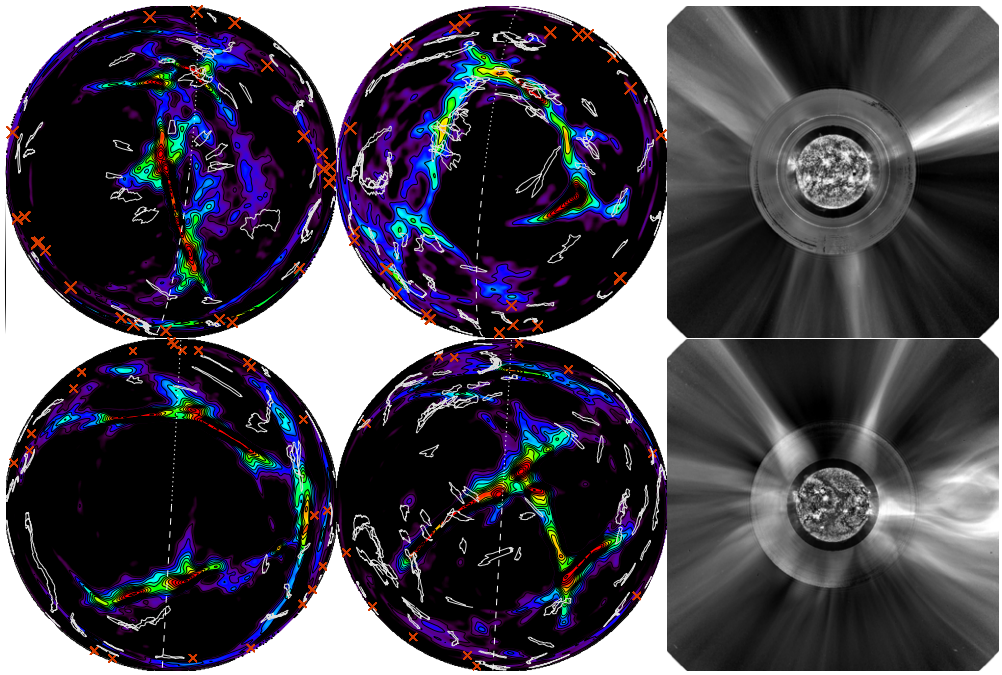

Figure 7. Polar density maps and coronal composite images for CR1961 (top row) and CR1970 (bottom row). The polar maps show the tomography density distribution as viewed looking down from the heliographic north pole (left plot) and up from the south pole (right plot). As with Figure 4, the dashed (dotted) white line in the density map shows the position of the west (east) limb at the time the coronal image is taken.

and two separated plasma sheets are isolated at high latitude. In the south, filaments are scattered at high latitude, and a band of high coronal density lies across the pole.

4.5. CR1988–CR2055: Descending Phase

Figure 8 shows a series of maps that summarizes the decline from solar maximum back toward a solar minimum configuration. CR1988 (2002/04) shows a return to a corona where there are no streamers above the poles, and the filaments and streamers share the same latitudinal extent. Plasma sheets are scattered throughout the corona, and the density structure is very complicated. Between CR1988 and CR2055, the corona slowly returns to a minimum-type. In contrast to the ascending phase, there is no rapid jump between a minimum and maximum configuration. Indeed, by CR2055 (2007/04), the corona has still not reached a minimum configuration—there are still dual plasma

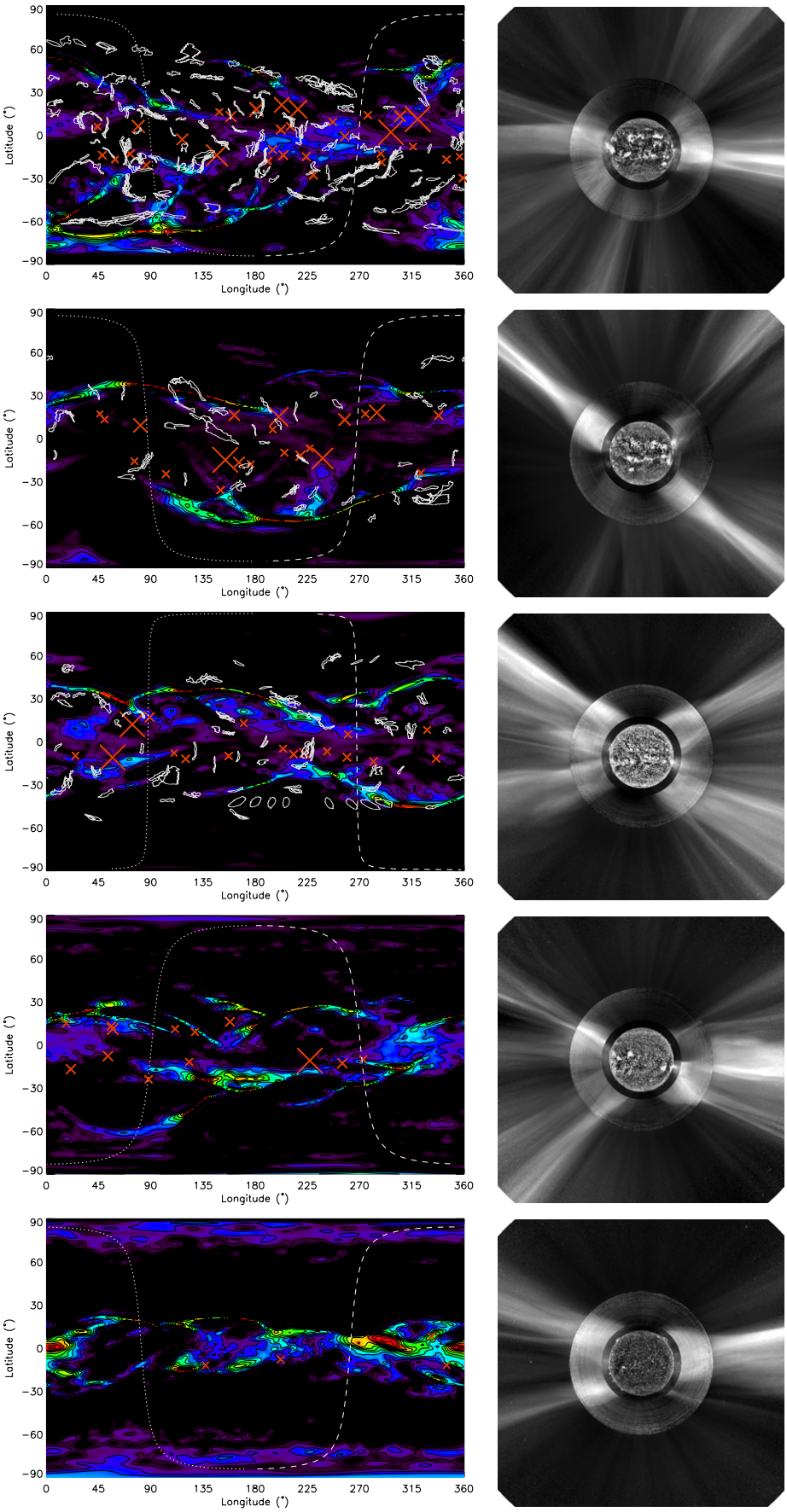

Figure 8. As Figure 4, but for CR1988 (2002/04), CR2002 (2003/04), CR2017 (2004/06), CR2033 (2005/08), and CR2055 (2007/04) (top to bottom). Unfortunately, we do not have access to filament data past 2004 December, so filaments are not shown for CR2033 and CR2055.

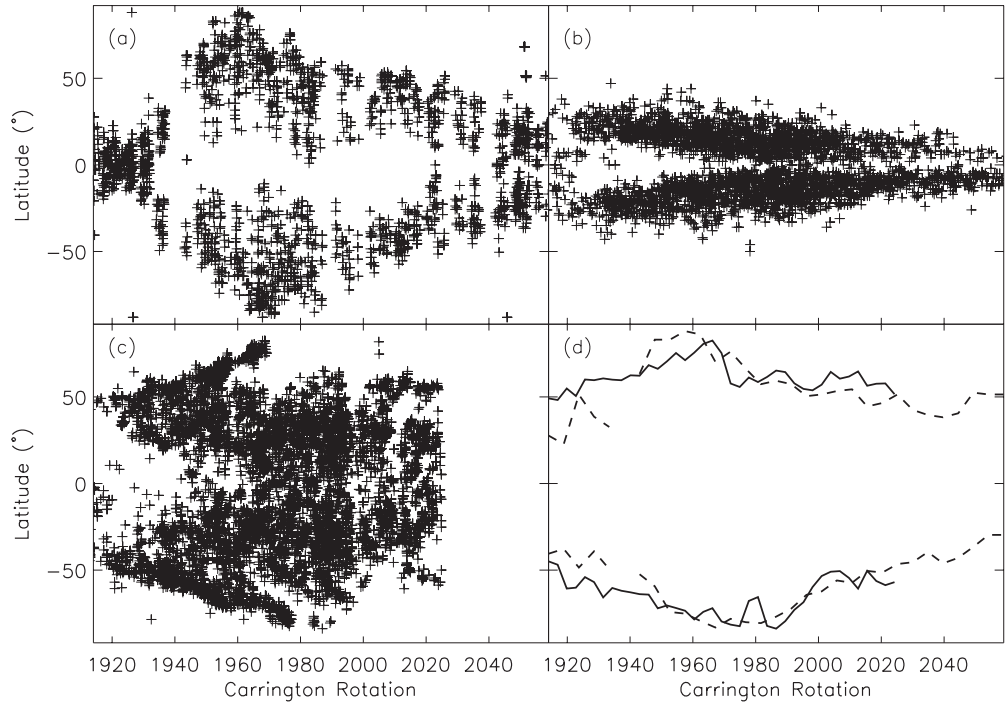

Figure 9. (a) Latitude of high-density peaks (streamers) as a function of time (or CR) over most of the last solar cycle. This was calculated for heights centered near 4 $R_{\odot}$ (or well into the height range where the corona becomes radial). The data gap near CR1940 was due to the loss of the *SOHO* satellite, and other rotations are missing due to data problems. The plot begins with CR1914 (1996/09/18) and ends at CR2058 (2007/07/18). The few outlying points should be ignored. (b) The latitude of active regions containing sunspots observed over the same time period as (a). Data from the Solar Region Summary archive was used (see acknowledgments). (c) The latitude of filaments observed from CR1914 to CR2024. Data from the Solar Feature Catalogue of the EGSO was used (Zharkova et al. 2005). The reduced filament data ends at December 2004. Only filaments with angular length larger than 15° are included. (d) Solid line: the maximum (minimum) observed latitude of filaments in the north (south). A sliding window of 1.5 Carrington rotations was used to calculate the maximum (or minimum). Dashed line: the same for streamers in the corona. Note that a point filter was used to remove the few outlying data points for the calculation of the sliding window maximum and minimum.

sheets in the north and south at all longitudes. Despite this, during CR2055, the streamers are seen to lean toward the equator rather than extend radially from their source regions. The streamer configuration of CR2055 is typical of a long period before solar minimum, spanning several years. The streamers are limited in latitude, but form dual bands of high density in both the north and south. The two bands of streamers arise from mid-latitude, and lean toward the equator.

5. CORONAL BUTTERFLY DIAGRAM

Figure 9(a) shows the latitudinal distribution of coronal high-density peaks over most of the last solar cycle. The coronal streamers are most closely concentrated to the equator (narrowest latitudinal distribution) during CR1921 (1997/04). Over a period of around three years following this solar minimum-type corona, the streamers migrate to the poles. There is an abrupt increase in latitude extent just after CR1930 (1997/12), particularly in the south. This is before the data gap caused by the loss of the *Solar and Heliospheric Observatory* (*SOHO*) satellite. A few streamers reach the north pole at CR1960 (2000/03), and the south pole during CR1965 (2000/07). The streamers then begin a steady migration back to mid-latitudes. At the end of the time period under study, they have not reached a distribution similar to the narrowest latitudinal spread seen in April 1997. The drift from the poles to the equator after year 2000 is far slower than the drift from the equator to the poles from years 1997 to 2000. The drift from maximum to minimum seems to halt in the north between CR1990 and 2020 (2002/06 to 2004/09), remaining stable at an approximately constant latitude for a long period.

Figure 9(b) shows a familiar time–latitude plot, or butterfly diagram, for photospheric active regions over the same time period as Figure 9(a). The latitudinal profile of streamers against time is in contrast to the latitudinal profile of active regions with time. Appreciable numbers of active regions appear at mid-latitudes just after CR1921, which coincides with the tightest equatorial concentration of coronal streamers. The active regions then describe a steady migration toward the equator throughout the period of time under study, while the streamers migrate to the pole and back down to mid-latitudes. It is clear, from Figures 9(a) and (b), that in general, high-density streamers at mid- to high latitudes in the extended corona are not radially centered above active regions—they tend to lie at higher latitudes than the bulk of active regions. At the nadir of solar minimum (CR1921), the streamers lie closer to the equator than the active regions, which tend toward mid-latitudes.

Figure 9(c) shows the latitudinal distribution of filaments observed on the Sun in Hα over the time period from CR1914 (1996/09) to CR2024 (2004/12). Only large filaments, with angular length longer than 15°, were considered. For each filament, an approximate average longitude and latitude was calculated as follows. The smallest rectangular box which can encompass the filament is given in pixel coordinates by the European Grid of Solar Observatories (EGSO) catalog. The pixel coordinates are converted into heliographic longitude and latitude. This figure shows that filaments have, approximately, the same latitudinal extent as coronal streamers. This is shown in Figure 9(d). There is a strong correlation between the minimum and maximum latitudinal spread of filaments and coronal streamers, particularly for the minimum latitudinal extent in

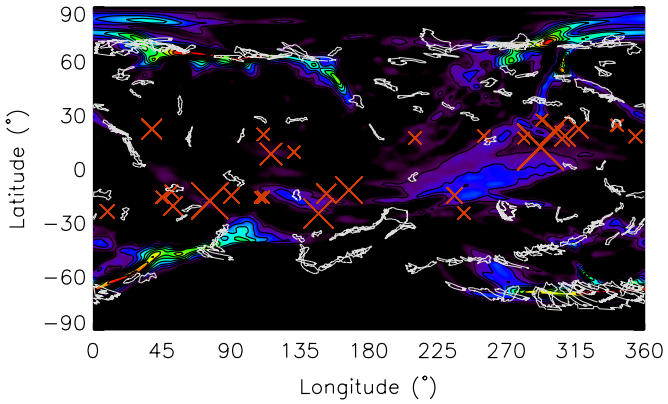

Figure 10. Tomographic reconstruction map for CR1955, with filaments overlaid as white contours, and active regions overlaid as red crosses.

the south. That is, they are both coronal features which are limited to the same latitudinal range over most of the solar cycle.

6. DISK AND CORONAL STRUCTURE OVER THE CYCLE

In general, there is a large latitudinal difference between active regions and the nearest streamer. This remains true for most of the solar activity cycle, suggesting that active regions are not the main structures underlying the largest and most stable streamers in the corona. Streamers do arise from active regions at low latitudes, but they are smaller, and less stable than large quiescent streamers at mid- or high latitudes. They are also unlikely to appear shaped as helmet streamers. Extended chains of active regions can lead to high-density sheet-like structures, which, when twisted, appear as fan-shaped streamers (Morgan & Habbal 2007b). These can remain structurally coherent over one or two rotations. All this does not mean that the large, quiescent helmet streamers are unconnected to active regions. Active regions are often seen forming the equatorial footpoints of large helmet streamers (see Morgan & Habbal 2007a), but the presence of the active region is not a prerequisite for the presence of the streamer. Smaller streamers arising from active regions can be bright, but if they are short-lived, they are less likely to be reconstructed by the tomography.

Filaments, on the other hand, seem to be more strongly linked to the quiescent, large-scale, and slowly changing streamer structure. The correlation between the latitudinal extent of filaments on the disk, and of streamers in the corona over the activity cycle shows that both phenomena are linked to the large-scale magnetic field configuration. Figure 10 is a good example of how streamers seem to overlie filaments on the disk. This is a period when the streamers arise radially from the disk, revealing the strong correlation between the distribution of filaments and coronal streamers. During solar minimum, this correlation is not seen directly since the streamers, arising from filaments (or the magnetic distribution underlying filaments), skew toward the equator. Therefore filaments are seen at mid-latitudes, while their associated streamers are forced by the large-scale coronal magnetic field to engulf the equator at a height of $\sim 3\ R_{\odot}$. The splitting of the plasma sheet seen in CR1912, stable for many rotations, could be interpreted as being caused by photospheric magnetic field activity near the equator associated with the final throes of the previous activity cycle, concentrated near longitude 270°. When the photospheric equatorial activity finally ends, the corona settles into a purely solar minimum configuration, with a single plasma sheet near the equator.

With the rise to solar maximum, and the splitting of the equatorial streamer sheet to two bands in the north and south, the streamers continue to skew somewhat to the equator, and therefore do not always appear at the same high latitudes as the filaments. By CR1955 (1999/10), the corona is approximately radial, and there is strong correlation in the distribution of streamers and high-latitude filaments. Between solar minimum and the radial streamer configuration of solar maximum, streamers arising from mid- and high-latitude photospheric structures deviate from the radial toward the equator, but do not reach and engulf it as they did during CR1922. The smaller helmet streamers formed above filaments and/or active regions at mid-latitudes do not merge together to form the huge equatorial-arching helmet streamers of solar minimum. The large-scale magnetic structure of the corona has changed, and allows the streamers to remain separated at most longitudes. The tomography results show that the transformation from a solar minimum-type corona to a solar maximum-type is rapid.

During solar maximum, and the ascending and descending phases, there seem to be two main contributions to the coronal streamer structure. There are the more stable quiescent streamers arising more or less radially from the high-latitude filaments, forming two bands of streamers in the north and south. The second contribution is streamer structure arising from the equatorial active regions. While these high-density streams can often diverge with height to join the helmet streamer structures at mid- or high latitude, they can also form their own separate streamers and contribute to the slow solar wind near the equator. These equatorial structures are not as stable as the quiescent streamers at higher latitudes. These two contributions to streamer structure often results in three bands of high density sharing the same longitude seen in the tomography maps, the best example extending over a large range of longitudes during CR1943, seen in Figure 6.

At solar minimum, and the rising phase of activity, the crown polar filaments are generally distributed at higher latitudes than the streamers. These filaments form the poleward footpoints of large helmet streamers which arch across the equator, or form smaller streamers which tend toward the equator. With the rising phase of activity, the butterfly diagrams of Section 5 show that streamers gradually occupy the same latitudinal extent as filaments. In the north corona during CR1943 (bottom plot of Figure 6), there is no clear correlation between filaments and streamers—large, extended plasma sheets lie above regions where there are no filaments. Since this can sometimes be seen during other rotations, streamers (or parts of streamer footpoints) must form above photospheric neutral lines regardless of the presence of filaments. The opposite is also true—filaments often form above photospheric neutral lines, and are not accompanied by coronal streamers. This is seen in the bottom plot of Figure 6, which shows the density configuration for CR1948. A band of filaments at high latitude in the south corona, extending from ∼270° to 90° (wrapping around the 360°), do not lie under streamers. Relevant to this discussion is the considerable differential rotation seen in the corona, introduced in Section 8. The presence of differential rotation, with a different rate to the photosphere, will introduce a twist in the coronal magnetic field, particularly at high latitudes. This adds uncertainty to making comparison between the distribution of filaments close to the Sun with streamers far from the Sun. Zhukov et al. (2008) shows that polar streamers are closely

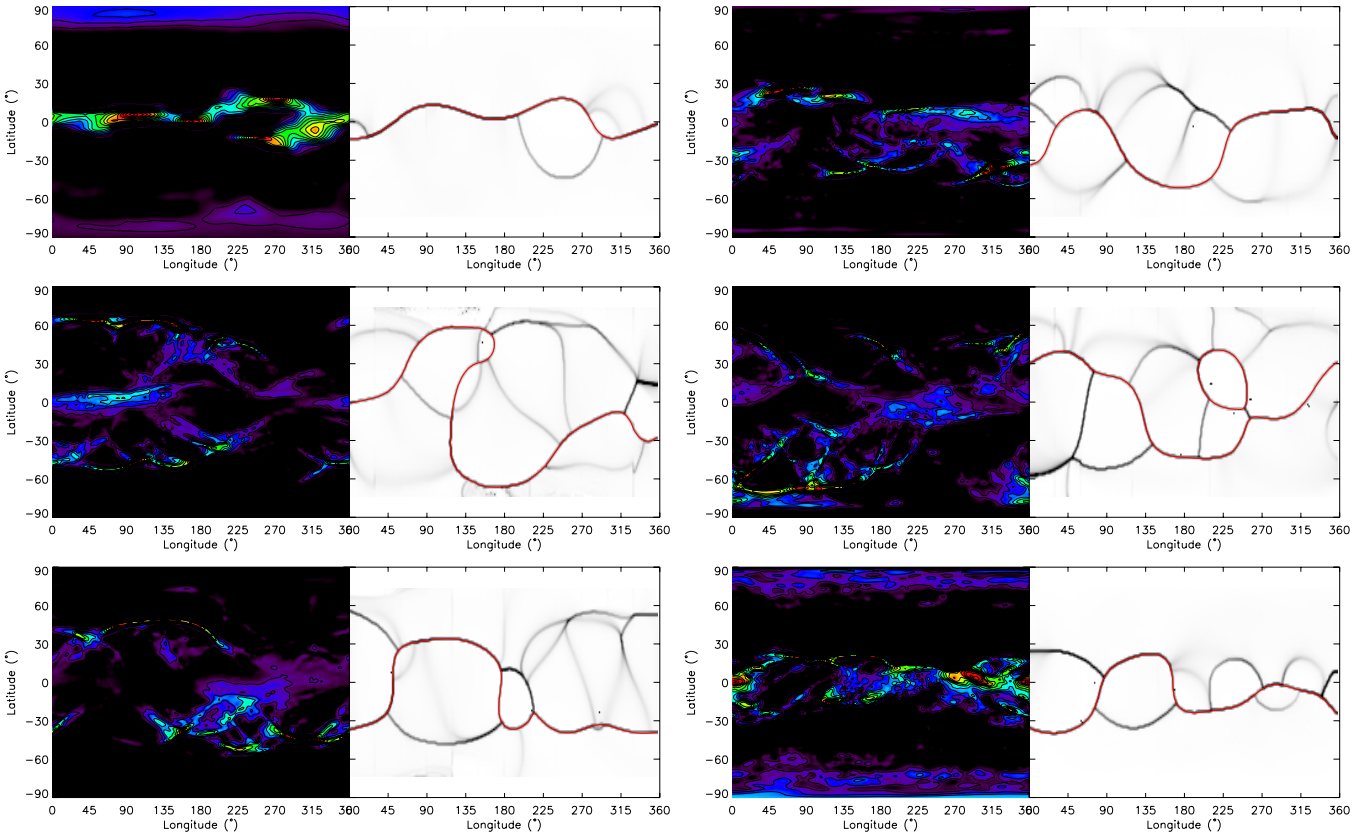

Figure 11. Comparison between tomography reconstructions and maps of average magnetic field line divergence from a potential field source surface (PFSS) model made at different times during the last activity cycle. From top to bottom: CR1912, CR1935, CR1943, CR1988, CR2010, and CR2055. In the PFSS maps, the dark lines indicate regions where field lines have diverged considerably from a radial path between the photosphere and the source surface (at a height of 3.25 $R_{\odot}$). The red line shows the heliospheric current sheet (HCS).

associated with what they call the "polar neutral lines," and are latitudinally centered above these lines at solar maximum. This is in good agreement with the findings of this study.

7. LINK WITH THE LARGE-SCALE MAGNETIC FIELD

The appearance of multiple plasma sheets that share the same extended longitudinal regions are strongly supportive of the "pseudostreamer" interpretation of PFSS magnetic models described by Wang et al. (2007). The model of Wang et al. (2007) allows multiple plasma sheets to arise from a potential field magnetic field configuration, not just the one high-density sheet associated with the HCS. Figure 11 shows several examples from the last activity cycle where the distribution of streamers revealed by tomography is compared to the results of PFSS. These extrapolations are based on observations of the photospheric magnetic field provided by the Wilcox Solar Observatory (see the Acknowledgments). The source surface is binned in 360 longitude bins (1°), and 180 latitude bins (also 1°). Field lines are traced from each point at the source surface down to the Sun. For each point on the source surface, the angular distance from that field line's source at the Sun to the source of its neighboring field lines is calculated. An average angular distance is then assigned to each point on the source surface. This is the value mapped in the PFSS maps of Figure 11. For brevity, we call this value convergence. High convergence values in the map show regions at the source surface where field lines have come from far-separated regions on the Sun. These regions form distinct lines on the longitude–latitude maps, or sheet-like surfaces in the 3D corona, which we call convergence sheets. If all the field lines come from the same locality at the Sun, the convergence is close to zero. This approach is similar to the technique described by Wang et al. (2007).

What is apparent from Figure 11 is the remarkable agreement between the distribution of high-density streamers calculated by tomography from coronal observations and the distribution of convergence sheets obtained from an extrapolation of photospheric measurements. We now give a comparison of each tomographic and convergence map shown in Figure 11.

CR1912 (1996/08). The splitting of the main streamer belt seen in the tomography map during CR1912 has a corresponding dual convergence sheet in the PFSS map. The north sheet contains the polarity reversal (distinguished by the red convergence sheet), and indeed, the tomography shows a more continuous and high-density structure along this sheet. The south convergence sheet is fainter and narrower. The PFSS map shows several weak convergence sheets not corresponding to any density structures in the tomography map.

CR1935 (1998/04). This is a corona recently developed into a solar maximum type (see Section 4.2). The tomography map shows a myriad of high-density structures, similar to the complicated distribution of sheets in the convergence map. The main HCS has two peaks and troughs, with corresponding density structure in the tomography map, at a reasonable spatial agreement. Between longitudes 225° and 360° in the south, there is good correspondence between density and convergence sheets. At other places, the spatial correspondence is not so good, although there is approximate topological agreement. The worst agreement is in the north at longitudes around 70°.

CR1943 (1998/12). The HCS has a complicated path between longitudes 0° and 180°, doubling back on itself in one place. Between 180° and 360°, it meanders in the south. It has corresponding density sheets in the corona, except for one region between 225° and 300°. It also meanders too far to the south compared to observation. In the north, between longitudes 180° and 315°, the convergence sheets are situated far to the north compared to observation, although there is again reasonable topological agreement. Lying along the north edge of the equator near 340° is a loop of convergence sheets, with a corresponding loop of high density in the corona. The three plasma sheet density configuration between longitudes 0° and 180°, discussed in Sections 4.3 and 6, is comprised of a complicated network of convergence sheets, with the sheet containing the polarity reversal forming part of the center equatorial sheet (0° and 45°) before branching into the mid-latitude north streamer belt.

CR1988 (2002/04). Considering the high activity of the solar maximum corona, there is good agreement between the CR1988 convergence and tomography maps. Topologically, the agreement is excellent, as the reader can establish from visual inspection. Spatially, the convergence sheets in the PFSS map occupy too small a latitudinal range. Streamers are restricted from −85° to 55°, while the corresponding convergence sheets only extend from −60° to 45°. There are other spatial discrepancies.

CR2010 (2003/12). This is a simpler distribution of streamers compared to CR1988. The HCS has overall a simple sine wave-like appearance, with corresponding density structure over most of its length. Other convergence sheets form a sine wave-like shape 180° out of phase with the HCS in longitude, most of which is not accompanied by streamers. Furnication sheets form a small, well-defined loop near 180° longitude, corresponding to a complicated cluster of density sheets, situated somewhat south and to higher longitudes than that predicted by PFSS.

CR2055 (2007/04). The convergence sheets are far more restricted in latitude, in agreement with the observed density structure. Between 0° and 180°, the HCS forms a sine wave-like shape, with good correspondence in streamer distribution. Similar to CR2010, non-HCS convergence sheets form an opposed phase sine wave-like shape at the same range of longitudes, with corresponding streamers. Between 180° and 360°, the HCS meanders just south of the equator, and convergence sheets describe relatively small loops branching off the HCS. The density maps show that the PFSS estimate of the HCS position is inaccurate, but complicated small-scale structure branching off the main high-density streamer sheet is in qualitative agreement with the convergence map.

High-density streamers are associated strongly with regions of high convergence. This is shown by the good topological agreement between the PFSS results and the tomography. However, there are considerable differences in the exact spatial distribution of streamers predicted by the two methods. The topological agreement is direct evidence of the basic correctness of the findings of Wang et al. (2007), and shows that PFSS models may be used to estimate the distribution of streamers, given the correct interpretation. However, there is a limit to the spatial accuracy of the PFSS model. In a comparison of *Ulysses* observations and a PFSS model, Neugebauer et al. (1998) also found large (up to 20°) latitudinal disagreement between the modeled position of the HCS and its measured value. Global MHD models may give improved agreement with the tomography maps, as was shown for one particular case in Morgan et al. (2009). Vásquez et al. (2008) gives detailed comparisons between tomography reconstructions and MHD models.

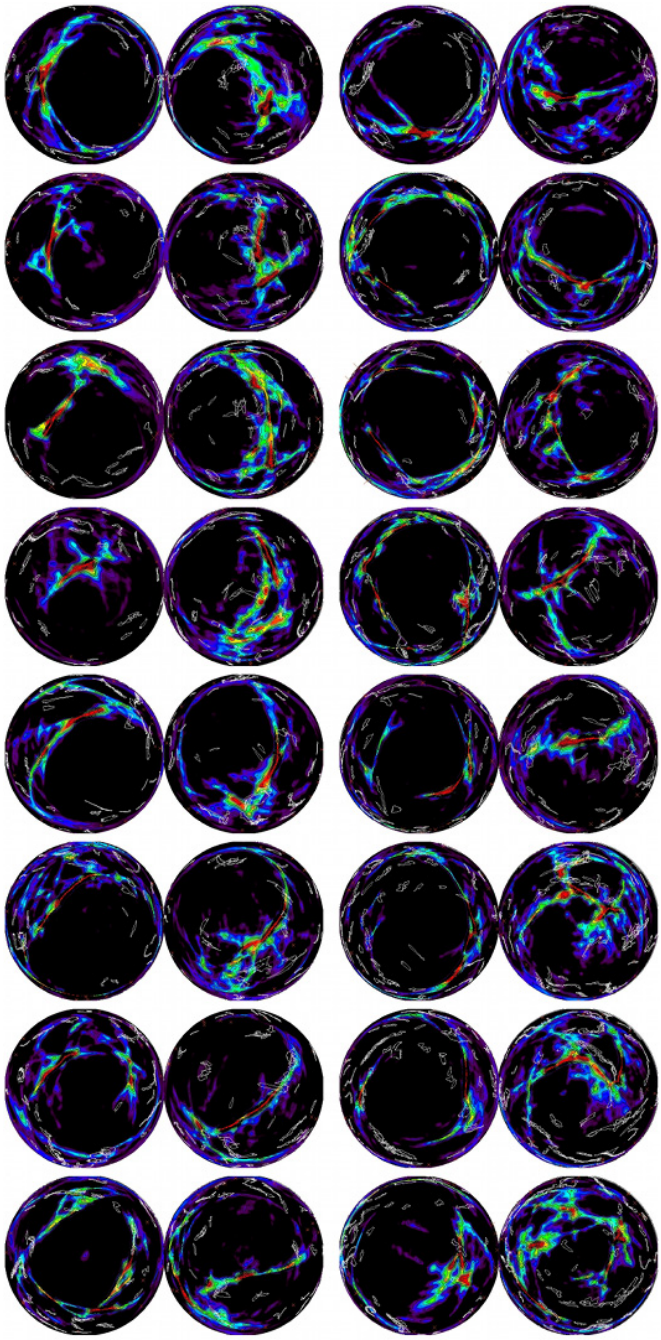

Figure 12. Sixteen polar map north–south pairs for consecutive CRs starting with CR1973 (top left), and ending with CR1989 (bottom left). The order is column major (consecutive rotations follow down the left column first, then down the right column). Each pair shows the view from the north pole (left) and south pole (right).

8. DIFFERENTIAL ROTATION

Although a correlation exists between the latitudinal extent of filaments and streamers, a longitudinal correlation is sometimes difficult to establish. Sometimes, a correlation seems obvious, as can be seen for rotation CR1961 at the south pole in Figure 7, or for the whole corona for CR1955 seen in Figure 10. However, the correlation does not necessarily last from rotation

to rotation. Figure 12 shows a series of polar maps from sixteen consecutive rotations close to the height of solar maximum, when streamers are close to the poles. What is immediately obvious is a systematic circular movement of structure from rotation to rotation around the poles. This rotation is a lag behind the standard CR rate, and is considerable, particularly near the poles. The rotation rate seems to be irregular, but this may be due to structures varying in latitude, and thus moving to a region of different rotation rate. A rough estimate of the structure movement in the north suggests a lag of around 17° per standard CR. This is estimated from the first five rotations shown in Figure 12. The rotation in the south is clearer, and a rotation lag of around 14° per standard CR is estimated. We stress that these are approximate values. A more rigorous analysis of the coronal differential rotation using tomography will be made in a separate study.

Lewis et al. (1999) made an estimate of the coronal rotation rate by applying a long-term autocorrelation analysis on LASCO data. In that case, the twin streamer configuration shown in Figure 4 near longitude 270°, which survived for several rotations, was used to establish a rotation rate. Their conclusion of a rigidly rotating corona is probably due to their measurement of a solar minimum corona, with streamers limited to low latitudes. Tomography allows an improved estimate of coronal differential rotation at all latitudes. Giordano & Mancuso (2008) used UVCS/*SOHO* data to establish rotational rates which differed with latitude, and also found that the differential rotation was not consistent between the north and south hemispheres. This is in agreement with the results of Figure 12. Wang et al. (1988) interprets the slow variation of large-scale coronal structure by the location of the (large-scale) nonaxisymmetric photospheric flux. Near solar minimum, this flux is concentrated near the equator, giving rise to a quasi-rigid coronal rotation at roughly the equatorial rate. Near solar maximum, the nonaxisymmetric photospheric flux is spread over a wide range of latitudes, giving rise to a slower and more differential coronal rotation. The presence of a considerable coronal differential rotation has implications for many areas of coronal research, including interpretation of in situ heliospheric measurements, and of coronal heating and acceleration mechanisms. The differential rotation makes any comparison of disk and coronal structure very complicated. Tomographic maps give direct observational evidence of this important process.

9. CONCLUSIONS

1. High-density coronal streamers are almost always very narrow sheets, extended in longitude, consistent with the idea of plasma sheets. At 4 $R_\odot$, the narrowest plasma sheet has a heliocentric angular thickness of approximately 2.°8.
2. Large-scale stable streamers are closely linked to the same large-scale photospheric magnetic configuration, which give rise to large filaments.
3. At most times outside the height of solar maximum, there are two separate stable large helmet streamer extending from mid-latitudes (in both north and south). At solar minimum, the streamers converge and join near the equator. Outside of solar minimum, the two streamers do not join, forming separate high-density sheets in the extended corona (one in the north and another in the south). During the ascending and descending activity phases, the streamers tend toward the equator, rather than rise radially from their source regions. At solar maximum, streamers rise radially from their source regions.
4. The poleward footpoints of the streamers are often above crown polar filaments, or above the photospheric neutral line which underlie the crown filaments. The equatorial footpoints of the streamers are above filaments or active regions, or above the photospheric neutral line which underlie these structures.
5. The high-density structures arising from the equatorial active regions either rise to become part of the equatorial footpoints of the mid-latitude quiescent streamers, or form unstable streamers at the equator, not connected to the quiescent streamer structure at mid- or high latitude (so there are often three plasma sheets sharing the same longitudinal region).
6. The corona seldom shows a simple single current sheet configuration. Two or even three high-density plasma sheets can share the same longitudinal region. This is inconsistent with the accepted single HCS configuration, but consistent with the idea of a density distribution formed of the main HCS and plasma sheets called pseudostreamers (Wang et al. 2007). A correct interpretation of PFSS models demands the inclusion of pseudostreamers: high-density sheets not necessarily associated with a magnetic polarity reversal, but rather with regions containing field lines arising from widely separated sources at the Sun.
7. There is an abrupt change from a solar minimum corona, where most of the streamers are confined to a single plasma sheet near the equator, to a maximum corona, where multiple plasma sheets sharing the same longitudes almost encircle the Sun. This happens between CR1931–CR1934. The descending phase from maximum to minimum is far more gradual. The corona still has a multiple plasma sheet configuration during CR2055.
8. Differential rotation in the corona (and on the disk) makes analysis and interpretation complicated—the corona is twisted, particularly above the poles. The presence of differential rotation has implications for many areas of coronal and heliospheric research.

10. FUTURE WORK

The tomography technique continues to be improved. Morgan & Habbal (2009) have recently developed a method to greatly reduce "contamination" by CMEs in coronal images, enabling a cleaner reconstruction of the corona. The use of STEREO SECCHI coronagraphs enable tomographic reconstructions to be made over a shorter time period than half a solar rotation. Whereas this study is based on one reconstruction per CR, a better approach would be a sliding window of reconstructions, where the half-solar rotation of data necessary for a reconstruction is slid forward in time increments of a day or so over a long time period. This will enable a far better analysis of differential rotation, for example. Improved connections between structures on the disk and streamers in the corona can be made by using appropriately reduced EIT, or STEREO Extreme UV Imager (EUVI) observations. Recent advances allow the automated detection of filaments in such observations (Scholl & Habbal 2008). Comparison of tomography results with PFSS model results is a very promising approach for unravelling the coronal structure at low heights. The tomography results confirm the accuracy of the PFSS model at the source surface, while the PFSS model provides a good estimate of the large-scale magnetic field below the source surface, allowing streamers to be traced back to their sources on the Sun.

This work is supported by NASA grant NNX07AH90G to the Institute for Astronomy. The *SOHO*/LASCO data used here are produced by a consortium of the Naval Research Laboratory (USA), Max-Planck-Institut fuer Aeronomie (Germany), Laboratoire d'Astronomie (France), and the University of Birmingham (UK). *SOHO* is a project of international cooperation between ESA and NASA. The active region data is extracted from the Solar Region Summary reports, prepared jointly by the US Department of Commerce, NOAA, Space Weather Prediction Center, and the US Air Force from data received by the Space Weather Operations branch of NOAA. The filament data is provided by L'Observatoire Paris Meudon. The Wilcox Solar Observatory's coronal field extrapolations were obtained from the WSO section of Stanford University's Web site courtesy of J. T. Hoeksema. WSO is supported by NASA, the NSF, and ONR.

REFERENCES

Altschuler, M. D., & Newkirk, G., Jr. 1969, Sol. Phys., 9, 131
Ambrož, P., Druckmüller, M., Galal, A. A., & Hamid, R. H. 2009, Sol. Phys., 258, 243
Banaszkiewicz, M., Axford, W. I., & McKenzie, J. F. 1998, A&A, 337, 940
Brueckner, G. E., et al. 1995, Sol. Phys., 162, 357
Carrington, R. C. 1858, MNRAS, 19, 1
Delaboudiniere, J.-P., et al. 1995, Sol. Phys., 162, 291
Frazin, R. A. 2000, ApJ, 530, 1026
Frazin, R. A., Kamalabadi, F., & Weber, M. A. 2005, ApJ, 628, 1070
Gibson, S. E., Foster, D. J., Guhathakurta, M., Holzer, T., & St. Cyr, O. C. 2003, J. Geophys. Res. (Space Phys.), 108, 7
Giordano, S., & Mancuso, S. 2008, ApJ, 688, 656
Guhathakurta, M., Holzer, T. E., & MacQueen, R. M. 1996, ApJ, 458, 817
Habbal, S. R., Morgan, H., Johnson, J., Arndt, M. B., Daw, A., Jaeggli, S., Kuhn, J., & Mickey, D. 2007, ApJ, 663, 598
Ko, Y.-K., Li, J., Riley, P., & Raymond, J. C. 2008, ApJ, 683, 1168
Kohl, J. L., et al. 1995, Sol. Phys., 162, 313
Koutchmy, S. L., Merzlyakov, V. L., & Molodenskii, M. M. 2001, Astron. Rep., 45, 834
Leamon, R. J., & McIntosh, S. W. 2009, ApJ, 697, L28
Lepri, S. T., Antiochos, S. K., Riley, P., Zhao, L., & Zurbuchen, T. H. 2008, ApJ, 674, 1158
Lewis, D. J., Simnett, G. M., Brueckner, G. E., Howard, R. A., Lamy, P. L., & Schwenn, R. 1999, Sol. Phys., 184, 297
Linker, J. A., et al. 1999, J. Geophys. Res., 104, 9809
Loucif, M. L., & Koutchmy, S. 1989, A&AS, 77, 45
Maunder, E. W. 1922, MNRAS, 82, 534
McIntosh, S. W., Davey, A. R., & Hassler, D. M. 2006, ApJ, 644, L87
Mikic, Z., Linker, J. A., & Colborn, J. A. 1996, BAAS, 28, 868
Morgan, H., & Habbal, S. R. 2007a, A&A, 464, 357
Morgan, H., & Habbal, S. R. 2007b, A&A, 465, L47
Morgan, H., & Habbal, S. 2009, ApJ, submitted
Morgan, H., Habbal, S. R., & Lugaz, N. 2009, ApJ, 690, 1119
Morgan, H., Habbal, S. R., & Woo, R. 2006, Sol. Phys., 236, 263
Neugebauer, M., Liewer, P. C., Smith, E. J., Skoug, R. M., & Zurbuchen, T. H. 2002, J. Geophys. Res. (Space Phys.), 107, 1488
Neugebauer, M., et al. 1998, J. Geophys. Res., 103, 14587
Pasachoff, J. M., Rušin, V., Druckmüller, M., Aniol, P., Saniga, M., & Minarovjech, M. 2009, ApJ, 702, 1297
Quémerais, E., & Lamy, P. 2002, A&A, 393, 295
Richie-Halford, A. C., Iess, L., Tortora, P., Armstrong, J. W., Asmar, S. W., Woo, R., Habbal, S. R., & Morgan, H. 2009, Space Weather, 7, 12
Saez, F., Llebaria, A., Lamy, P., & Vibert, D. 2007, A&A, 473, 265
Saez, F., Zhukov, A. N., Lamy, P., & Llebaria, A. 2005, A&A, 442, 351
Saito, K., Poland, A. I., & Munro, R. H. 1977, Sol. Phys., 55, 121
Schatten, K. H., Wilcox, J. M., & Ness, N. F. 1969, Sol. Phys., 6, 442
Scholl, I. F., & Habbal, S. R. 2008, Sol. Phys., 248, 425
Starck, J.-L., Murtagh, F., & Bijaoui, A. 1998, in Image Processing and Data Analysis. The Multiscale Approach, ed. J.-L. Starck, F. Murtagh, & A. Bijaoui (Cambridge: Cambridge Univ. Press)
Stone, E. C., Frandsen, A. M., Mewaldt, R. A., Christian, E. R., Margolies, D., Ormes, J. F., & Snow, F. 1998, Space Sci. Rev., 86, 1
Susino, R., Ventura, R., Spadaro, D., Vourlidas, A., & Landi, E. 2008, A&A, 488, 303
Thernisien, A. F., & Howard, R. A. 2006, ApJ, 642, 523
Usmanov, A. V. 1996, in AIP Conf. Ser. 382, A Global 3-D MHD Solar Wind Model with Alfvén Waves, ed. D. Winterhalter, J. T. Gosling, S. R. Habbal, W. S. Kurth, & M. Neugebauer (Melville, New York: AIP), 141
Uzzo, M., Strachan, L., Vourlidas, A., Ko, Y.-K., & Raymond, J. C. 2006, ApJ, 645, 720
van de Hulst, H. C. 1950, Bull. Astron. Inst. Neth., 11, 135
Vásquez, A. M., Frazin, R. A., Hayashi, K., Sokolov, I. V., Cohen, O., Manchester, W. B., IV, & Kamalabadi, F. 2008, ApJ, 682, 1328
Wang, Y.-M., & Sheeley, N. R., Jr. 1990, ApJ, 355, 726
Wang, Y.-M., & Sheeley, N. R., Jr. 1992, ApJ, 392, 310
Wang, Y., Sheeley, N. R., Jr., Nash, A. G., & Shampine, L. R. 1988, ApJ, 327, 427
Wang, Y.-M., Sheeley, N. R., Jr, & Rich, N. B. 2007, ApJ, 658, 1340
Wang, Y.-M., et al. 1997, ApJ, 485, 875
Wenzel, K. P., Marsden, R. G., Page, D. E., & Smith, E. J. 1992, A&AS, 92, 207
Zharkova, V. V., Aboudarham, J., Zharkov, S., Ipson, S. S., Benkhalil, A. K., & Fuller, N. 2005, Sol. Phys., 228, 361
Zhou, X.-Y., Smith, E. J., Winterhalter, D., McComas, D. J., Skoug, R. M., Goldstein, B. E., & Smith, C. W. 2005, in ESA Special Publication 592, Solar Wind 11/*SOHO* 16, Connecting Sun and Heliosphere, ed. B. Fleck, T. H. Zurbuchen, & H. Lacoste (ESA SP-592; Noordwijk: ESA), 659
Zhukov, A. N., Saez, F., Lamy, P., Llebaria, A., & Stenborg, G. 2008, ApJ, 680, 1532